Research article

Influence of the pH of anthocyanins on the efficiency of dye sensitized solar cells

Alex Okello [a],[*], Brian Owino Owuor [b], Jane Namukobe [c], Denis Okello [a], Julius Mwabora [b]

[a] *Department of Physics, Makerere University, P.O. Box 7062, Kampala, Uganda*
[b] *Department of Physics, University of Nairobi, P.O. Box 30197-00100, Nairobi, Kenya*
[c] *Department of Chemistry, Makerere University, P.O. Box 7062, Kampala, Uganda*

A R T I C L E   I N F O

A B S T R A C T

The influence of the pH of anthocyanins on photovoltaic performance in dye-sensitized solar cells has been investigated. Anthocyanins were extracted from crushed leaf stocks of *Manihot esculenta* Crantz (Cassava plant) using methanol acidified with 0.5% trifluoracetic acid. The filtrate was concentrated using a rotary evaporator and partitioned against ethyl acetate. The anode was prepared by screen printing TiO_2 paste on a previously cleaned fluorine-doped tin oxide (FTO) glass substrate. The cathode was made by applying plastisol on a previously cleaned FTO glass substrate using an artistic brush and later annealed at 450 °C for 20 min to activate platinum. The performance of the solar cells was measured using a solar simulator fitted with an AM1.5 air filter. Electron transport was studied using electrochemical impedance spectroscopy (EIS). It was observed that the short circuit current and efficiency dropped from pH 2 to pH 6 and peaked at pH 8, with values of 0.399 mA and 0.390%, respectively. It then drops further as the basicity increases. The open circuit voltage was observed to increase consistently from pH 2 to pH 12. EIS results showed that the electron density in the conduction band of TiO_2 increases from pH 2 to pH 10 and drops from pH 10 to pH 12. It was concluded that, while a large number of electrons ($\sim 10^{16} m^{-3}$) are injected into the conduction band of TiO_2, the majority do not contribute to the current but instead recombine with other electron acceptor species in the solar cell. However, the injected electrons cause an upwards shift in the quasi-Fermi level of electrons in the conduction band of TiO_2. This explains the large variation in the open circuit voltage compared to the short circuit current.

1. Introduction

The ever-diminishing fossil energy sources due to increased demand for energy and the need to mitigate the effects of pollutants emitted by fossil fuels on the environment have put a huge burden on scientists to find alternative sources of energy [1, 2, 3, 4]. This has led to a search for alternative sources of energy that are not only inexhaustible but are also environmentally benign [2, 3, 5]. An area that is currently being extensively researched is photovoltaic technology (PV) [1, 3]. This is attributed to the abundancy and eco-friendliness of solar energy technology [3, 4, 5, 6]. As of 2017, there were over twenty-four photovoltaic technologies [1]. Some of the technologies include polymer solar cells, perovskite solar cells, quantum dot solar cells, silicon photovoltaic solar cells, organic solar cells, tandem cells, dye sensitized solar cells (DSSC), and many others [1, 3]. Solar cell technologies have advantages and disadvantages [1]. DSSC is widely researched because its materials

are cheaper and easier to manufacture than those of other technologies [3, 6].

Discovered inadvertently in 1991 by Gratzel and coworkers [3, 7], the basic structure of the DSSC consists of an anode made of nanostructured TiO_2, given the sense of light by soaking in a dye [8]. The cathode is made of platinum, and the hole carrier is usually a redox couple [3]. The electrode materials are usually deposited on conducting glass substrates such as fluorine-doped tin oxide (FTO) or indium tin oxide (ITO) [3]. The glass substrates in addition to supporting the electrode materials also provide cell contacts [9].

When exposed to light, the dye, anchored onto TiO_2, absorbs light. As a result, electrons are excited and migrate from the Highest Occupied Molecular Orbital (HOMO) to the Lowest Unoccupied Molecular Orbital (LUMO) of the dye [10]. The attachment of the dye onto TiO_2 provides a pathway for electron injection into the conduction band of TiO_2 [4]. The injected electrons move through TiO_2 to the conducting glass substrates

---

and eventually to the counter electrode. At the same time, the electrolyte donates an electron to the dye, compensating for the electron that was injected into the conduction band. The electrolyte then receives another electron from the counter electrode, a process that is catalysed by platinum [9, 11].

Because of its huge potential to cheaply address the imminent energy crises and effects of fossil fuels on the environment, there has been considerable research worldwide on dye-sensitized solar cells [5]. Khalid *et al* investigated the effect of dye extracting solvent and dye absorption time on solar cell performance [12]. In their report, solar cells for which dyes were extracted with methanol had a solar conversion efficiency of 0.31%, while solar cells for which the dye was extracted with ethanol had a solar conversion efficiency of 0.32%. In addition, a dye adsorption time of 2 hours gave a solar conversion efficiency of 0.32%, while an adsorption time of 1 hour gave a solar conversion efficiency of 0.27%. Setyawati and coworkers investigated the effect of mixing Fe(III) in chlorophyll and then used the resultant mixture as a sensitizer [13]. The Fe(III)-chlorophyl sensitizer gave a solar conversion efficiency of 1.35%. With chlorophyl alone as a sensitizer, the solar cell efficiency was 0.7%. Golshan and colleagues investigated the effect of cosensitization in dye-sensitized solar cells using dye extracts from *Malva verticillate* and *Syzygium cumini* [14]. The solar cells obtained had efficiencies of 0.05% and 0.03% for *Malva verticillate* and *Syzygium cumini,* respectively. The dye cocktail gave an efficiency of 0.05% in an alkaline medium and 0.6% in an acidic medium. The better performance in acidic medium was attributed to less steric hindrance and multiple anchor groups to the TiO_2 surface. Tadesse and colleagues [15] studied the performance of dye extract from *Syzgium guineense*. The extract contained anthocyanins, among other pigments. They reported a solar conversion efficiency of 0.51%. In another study, Chien and Hsu [16] used anthocyanin extracts from red cabbage in dye-sensitized solar cells. They investigated the conditions that would maximize solar cell performance. They reported that the best performance was at pH 8, at a concentration of 3.0 mM. The solar conversion efficiency obtained was 1.4%.

While previous studies [15, 16] explored the performance of anthocyanins in dye-sensitized solar cells, they did not explain the performance in terms of electron density in relation to different molecular forms exhibited by anthocyanins in different pH environments. Additionally, in our previous study, we investigated the influence of the concentration of anthocyanins on electron transport in dye-sensitized solar cells at a constant pH of the sensitizing anthocyanins [9]. Improvement in photovoltaic performance as the concentration of anthocyanins increases was observed. The improved performance was attributed to the increased charge density, which increased concomitantly with increased light absorption as a result of the increased concentration of anthocyanins. We further reported that the increased charge density shifted the quasi-Fermi level of electrons in the conduction band of TiO_2, and in effect, the open circuit voltage increased with increasing anthocyanin concentration.

In the present study, we fixed the concentration of anthocyanins and varied the pH of the concentrated anthocyanins. Anthocyanins at various pH values but fixed concentrations were then used to sensitize solar cells. The influence of pH on photovoltaic performance was then evaluated. Electron transport in the solar cells was further investigated using impedance electron spectroscopy. We believe that knowledge of how the pH of anthocyanins influences performance in dye-sensitized cells is crucial in designing new dyes, electrolytes, anode and cathode materials for application in dye-sensitized solar cells.

2. Experimental part

HPLC grade methanol, ethyl acetate, acetone, 2-propanol, and trifluoracetic acid were purchased locally. Liquid electrolyte (Iodolyte AN-50), platinum catalyst (plastisol T/SP), fluorine-doped (FTO) oxide glass substrate ($7\Omega^2$), and hot melt sealing film meltonix (60 μm) were purchased from Solaronix SA. Kerocyanin chloride, liquid detergent, Helmanex III, commercial TiO_2 nanopowder (Degussa P25) comprising approximately 30% rutile, 70% anatase, Triton X-100, glass wool and polyethylene glycol (M. W 10,000) were purchased from Sigma Aldrich Co.

2.1. Anthocyanin extraction and characterization

Leaves of *Manihot esculenta* Crantz (cassava leaves) were picked from a garden in Lira in the northern part of Uganda and taken to Makerere University Herbarium, Department of Plant Science, Microbiology and Biotechnology for confirmation. Leaf stocks were detached from their leaves, chopped into small pieces with a knife and crushed in an agate *mortar* before macerating in 680 ml of methanol acidified with 0.5% trifluoracetic acid for 24 h. This was kept in a deep freezer set at -20 °C [17].

The soaked leaf stocks were sieved and filtered with a funnel fitted with glass wool to obtain 430 ml of the filtrate. The filtrate was concentrated using a rotary evaporator to 62 ml and partitioned against ethyl acetate. The lower layer containing mainly anthocyanins was recovered and concentrated using a rotary evaporator again to remove the residue ethyl acetate [18, 19]. The final volume of 62 ml was made to 300 ml using methanol acidified with 0.5% trifluoracetic acid. This was then divided into six portions of 50 ml each and placed in amber bottles. Their pH was adjusted to pH 2, pH 4, pH 6, pH 8, pH 10 and pH 12 using 3 M sodium hydroxide solution and concentrated hydrochloric acid. Measurement of pH was performed using a digital pH metre.

The absorption properties of the anthocyanins were measured in the spectral range of 380 nm–800 nm using a single beam Jenway 7315 spectrophotometer.

2.2. Preparation of electrodes and assembly of solar cells

Cleaning of FTO glass substrates, deposition of platinum and preparation of titanium paste were performed following the procedure in our previous work [9]. Briefly, FTO glass substrates were first cleaned using a 1% solution of Helmanex III in an ultrasonic bath for 20 min and rinsed three times with deionized water. Later, the electrodes were bathed in an ultrasonic bath of acetone for 20 min and 2-propanol for 20 min.

To prepare titanium paste, 4 g of commercial TiO_2 nanopowder, 8 ml of 0.1 *M nitric* acid solution and polyethylene glycol and Triton X-100 were blended and ground in an agate mortar to form a paste [20]. The cathode was prepared by applying plastisol, a platinum precursor, onto an FTO glass substrate using an art brush dipped in plastisol. The cathode was then annealed at 450 °C in a tube furnace (Labtech, model LEEF-4025-3) for 20 min and left to cool naturally in air.

The anode was prepared by screen printing TiO_2 paste on the previously cleaned FTO glass substrates. Briefly, a 61–64 screen-printing mesh was used in the process. The aperture of deposition on the mesh was 36 mm^2. The screen-printing mesh was placed on top of the pre-cleaned conducting side of the FTO glass substrate. Approximately 1gram of the previously prepared TiO_2 paste was scooped up with a plastic spatula and put into the aperture of the screen-printing mesh. A squeegee was used to disperse the paste through the mesh aperture onto the FTO glass. The deposited paste was left to spread uniformly for about 10 min, and transferred to a hot plate set at 120 °C for 10 min. This was to ensure that the deposited paste sticks to the FTO glass substrate. The procedure of screen printing was repeated two more times. The thickness of the deposited TiO_2 material was measured using a step surface profiler (Alpha-Step 500 Profiler, Tencor) and found to be of thickness 9.5μm. Annealing was performed at 450 °C in an open-air tube furnace for 20 min. When it had cooled to approximately 30 °C, the anodes were dipped in anthocyanins at varying pH values and left to absorb the anthocyanins for 16 h.

The dye-loaded anodes were washed with ethanol and placed with the conducting side facing up. Two pieces of Meltonix cut with a hole of approximately 8 mm by 8 mm were stacked and placed such that the deposited TiO_2 was within the hole. The prepared counter electrode was

placed on top of the anode so that contacts to the solar cells were sufficient for connecting crocodile clips. Sealing was performed using a hot solder iron pressed on top of the counter electrode along the edges of the solar cell. The electrolyte, iodolyte-AN 50, was injected into two holes behind the counter electrode, and the holes were sealed with cell cups and meltonix as before.

2.3. Photovoltaic measurements and electrochemical impedance spectroscopy

Absorbance measurements of the prepared anthocyanins were performed using a Jenway spectrophotometer, Model 7315. Photovoltaic performance was measured using a Keithley instrument (Model 2400, 4046884, C32) with the intensity of light set at 1000 Wm^{-2}. The open circuit voltage (V_{oc}), short circuit current (I_{sc}), and fill factor (FF) were measured. The solar conversion efficiency was computed using the relation [1]; (%) = $V_{oc} \times I_{sc} \times FF \times 100/P_{in}$; V_{oc} is the open circuit voltage, I_{sc} is the short circuit current, FF is the fill factor, and Pin is the power incident onto the solar cell [21].

Electrochemical impedance spectroscopy (EIS) was performed using an Autolab PGSTAT 204. A voltage of 0.7 V was applied to the solar cells, and the frequency was set to vary from 1 Hz to 1 MHz.

To fit the impedance data, the solar cells were simulated using the circuit of Figure 1, a simplified transmission line model, which represents physical processes and charge kinetics that take place in the solar cell. In the circuit, R1 is series resistance due to connecting wires, sheet resistance of glass substrates used, and any other materials that contribute serially to resistance. R2 is the charge transfer resistance at the counter electrode.

R3 is the charge transfer resistance associated with recombination at the TiO2/electrolyte interface [22], and C3 is the chemical capacitance due to the double layer at the anode. It is a measure of the ability of an electrochemical system to accept or release more charge as a result of variation in its Fermi level [23]. Q2 is a constant phase element (CPE) that was preferred to address the nonideality behaviour of the experimental data. The impedance of a CPE is given by [22] $Z_{CPE} = 1/Q(i\omega)^n$, where $i = \sqrt{-1}$, ω is the angular frequency, and Q has a magnitude with units of $F \times s^n$; $0 \leq n \leq 1$ such that when $n = 0$, the CPE behaves like an ideal resistor, and when $n = 1$, the CPE behaves like an ideal capacitor [24, 25]. When the CPE is connected in parallel with a resistor, its capacitance can be calculated using $C = (QR)^{1/n}/R$. Fitting was performed using RelaxIS3 software.

3. Results and discussion

3.1. Absorption properties of anthocyanins at different pH values

Figure 2 illustrates the absorption properties of anthocyanins at different pH values.
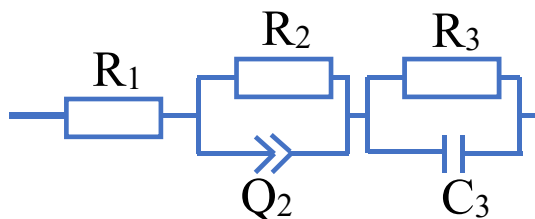
Figure 1. Simplified transmission line model. R$_1$: series resistance, R$_2$: charge transfer resistance of the counter electrode, R$_3$: charge transfer resistance of the anode, C$_3$: chemical capacitance at the anode, Q$_2$: constant phase element at the cathode.

The visible absorbance peaks for this sample are in the range of 500 nm–550 nm. As the pH increases from pH 2 to pH 12, the magnitude of the peaks decreases. Additionally, at higher pH values (pH 10 and pH 12), observable peaks at approximately 630 nm are present. It is worth noting, however, that due to the high concentration of anthocyanins used, the absorbance peaks below 460 nm are not visible.

Chine & Hsu, 2013 [16] reported similar results to the present study. For example, they observed absorption peaks in the range 300 nm–350 nm and 500 nm–550 nm. As pH increases, the peaks between 500 and 550 nm shift towards 600 nm and decrease in magnitude. In addition, the absorbances at the peaks were also in the order pH 2 > pH 4 > pH 6. At pH 8, there were two peaks at approximately 600 nm and between 300 nm and 350 nm. pH 10 and pH 12 have peaks at approximately 600 nm and 350–400 nm, respectively.

In contrast to the absorption properties of anthocyanins at varying concentrations, we reported a consistent increase in absorbance as the concentration increased, in accordance with the Lambert–Beer law [9]. This is different from the absorption properties of Figure 2 that have been described in the preceding paragraphs. The absorption properties are attributable to the different molecular forms of anthocyanins at different pH values. The molecular forms are explained as follows:

When anthocyanins are dissolved in water, their aglycones exhibit five distinct molecular forms that are in equilibrium with one another [19, 26]. Red flavylium cation, colourless carbino pseudo base, purple quinoidal base, blue quinoidal anion, and yellowish chalcone are the five molecular forms. The colour and equilibrium shift to a particular molecular form depending on the pH of the aqueous solution [19, 27].

At pH values less than 2.0, the flavylium cation takes precedence [19, 27]. The solution is red in colour. Deprotonation occurs when the pH is increased to between 4 and 6, resulting in the formation of a quinoidal base. At pH 4.0, the deprotonated aglycone is magenta in colour; at pH 6.0, it is purple. The quinoidal base loses another proton at pH 7.0, forming a blue quinoidal anion. When the pH is increased above pH 8, the flavylium cation dehydrates, forming a colourless carbinol pseudo base [19, 27]. Later, a yellow chalcone is formed. At a pH greater than 10.0, the green colour of the solution is a result of a mixture of blue quinoidal anion and yellow chalcone. These different molecular forms were not present in our previous studies on the influence of the concentration of anthocyanins on electron transport in dye-sensitized solar cells because the pH was fixed [9].

3.2. Influence of the pH of anthocyanins on the PV performance

An investigation was conducted into the photovoltaic performance of the solar cells sensitized using anthocyanins at various pH values. The performance parameters of solar cells fabricated with anthocyanins at various pH values are summarized in Table 1.

As observed in Table 1, the open circuit voltage increases from 0.476 V at pH 2 to 0.639 V at pH 12. Between pH 2 and pH 6, the short circuit current, fill factor, and efficiency decrease as the acidity of anthocyanins decreases. At pH 2, the short circuit current, fill factor, and efficiency were 0.322 mA, 0.638, and 0.272 %, respectively. The short circuit current, fill factor, and efficiency all decreased to 0.311 mA, 0.586, and 0.231%, respectively, at pH 6. At pH 8, the short circuit current and solar conversion efficiency were both at their maximum values of 0.399 mA and 0.390%, respectively. At pH 12, the current and efficiency values decrease to 0.278 mA and 0.260%, respectively. The fill factor reaches a maximum of 0.661 at pH 10 and then drops to 0.600 at pH 12. The variations are more easily observed in Figure 3, which illustrates the effect of pH on conversion efficiency.

Tadesse *et al.* [15] previously reported a similar trend. They studied dye-sensitized solar cells sensitized using dye extracts from *Sizygium guineas*. pH 0.5, pH 1.0, pH 2.0, and pH 3.3 were considered. Solar conversion efficiencies of 0.23%, 0.35%, 0.32%, and 0.30%, respectively, were achieved. The open circuit voltage and current followed a similar trend to that shown in Table 1.
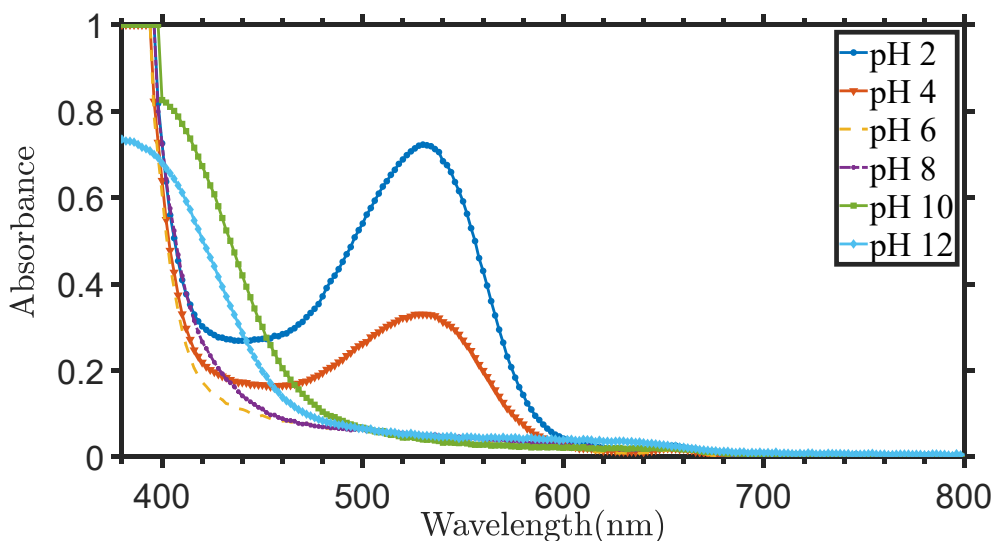
Figure 2. UV–VIS absorption spectra of anthocyanin extracts at varying pH values.

Table 1. Performance parameters for anthocyanin-sensitized solar cells at different pH values, Voc: Open circuit voltage, I_{sc}: Short circuit current, FF: Fill factor, η: Solar conversion efficiency.

	V_{oc}(V)	Isc(mA)	FF	η(%)
pH 2	0.476	0.322	0.638	0.272
pH 4	0.505	0.319	0.586	0.262
pH 6	0.536	0.311	0.498	0.231
pH 8	0.557	0.399	0.632	0.390
pH 10	0.593	0.275	0.661	0.299
pH 12	0.639	0.278	0.600	0.266

Suyitno *et al.* [28] used benzoic acid to acidify dye extracts from papaya leaves. Later, acidified dyes with pH values of 3.0, 3.5, 4.0, 4.5, 5.0, and 5.5 were used to sensitize solar cells. The efficiency values observed were 0.26%, 0.28%, 0.21%, 0.17%, and 0.11%. The trend of these observations in the pH 3.5–5.5 range is comparable to the trend shown in Table 1. The open circuit voltage and current also followed the same trend as in Table 1.

In another report, scandium/HOMBIKAT electrodes were synthesized [29]. The resulting electrodes were used to construct dye-sensitized solar cells, which were then sensitized using Rose Bengal dye at different pH values. The maximum efficiency of 10.34% obtained was at pH 8.4. In order of magnitude, the next highest efficiency obtained was 6.71% at pH 6.4.

To explain the trend shown in Figure 3, we consider the absorbance exhibited by anthocyanins at various pH values along with their different molecular forms.

In terms of photovoltaic performance at various pH values, the performance of the solar cells in the acidic region is in the order pH 2 > pH 4 > pH 6, which corresponds to the order of magnitude of the peaks in the absorbance spectrum of Figure 2, in the region 500 nm–550 nm. This means that the amount of light (photons) absorbed at various pH values has an effect on the performance of solar cells. When more photons are absorbed, presumably on the order of magnitude of the peaks in Figure 2, more electrons are excited and injected into the conduction band of TiO_2 [30]. This results in an increase in current and a general increase in the solar conversion efficiency. The increase in current as a result of increased absorption of photons was also observed in our previous
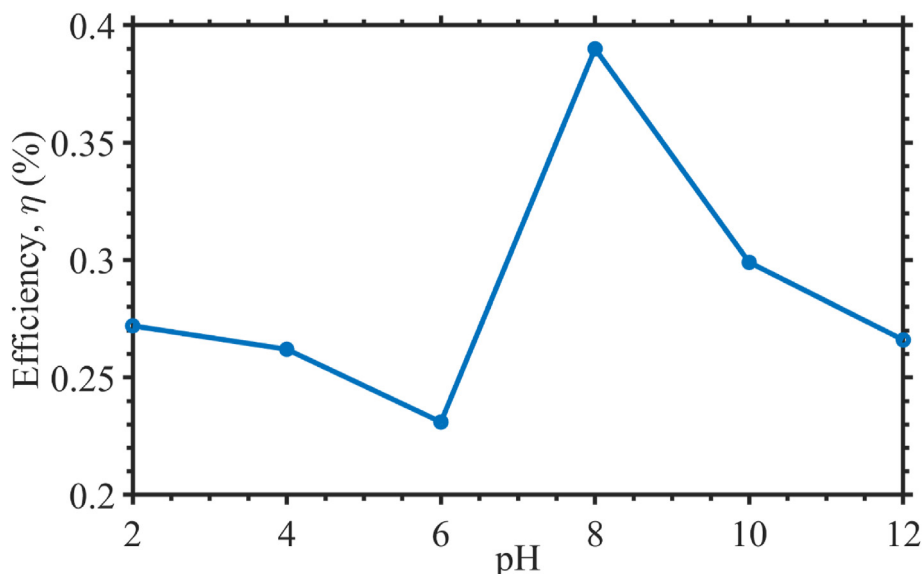
Figure 3. Graph showing the influence of pH on the solar conversion efficiency.

studies on the influence of concentration on electron transport in dye-sensitized solar cells [9]. While in the present study, increased absorption was attributed to different molecular forms of anthocyanins in different pH environments, our previous studies attributed the increase in absorption to an increase in the concentration of anthocyanins. In the next section, we demonstrate how changes in pH lead to increased charge density using impedance spectroscopy.

At pH 8, the highest short circuit current is most likely due to the optimal attachment of anthocyanins to the TiO2 surface when they are in the form of a quinoidal anion. This enables a more efficient transfer of electrons from the lowest unoccupied molecular orbital (LUMO) of the dye to the conduction band of TiO2 [31,27]. The short-circuit current decreases significantly at pH 10 and pH 12. This is probably due to poorer attachment of anthocyanins and the TiO2 surface. Deattachment of dye molecules from TiO2 has been reported at approximately pH 9 [3].

To explain the variation in open circuit voltage, we look at the open circuit voltage definition, as defined by Eq. (1) [32].

$$V_{oc} = \frac{E_{CB}}{e} - \frac{kT}{e}\ln\left(\frac{n}{N_{CB}}\right) - \frac{E_{redox}}{e} \qquad (1)$$

where n denotes the number of electrons in the conduction band of TiO2, N_{CB} denotes the effective density of states, e denotes the electron charge, E_{CB} denotes the conduction band edge of TiO2, and E_{redox} denotes the HOMO level of the electrolyte used.

According to Eq. (1), there are three ways to increase the open circuit voltage: (1) the negative shift in the conduction band edge, E_{CB} of TiO2, and (2) the positive shift in the HOMO of the redox couple. (3) Increasing the value of n [32]. In the present case, variations in the pH of anthocyanins mainly affect the second term on the right hand side of equation (1) as follows:

In TiO2, the number of electrons n in the conduction band of TiO2 is always less than the density of states N_{CB} [9]. This makes the term $kT/e \ln(n/N_{CB})$ on the right-hand side of Eq. (1) **to** always become negative [31]. When the solar cell (dye) absorbs photons of sufficient energy, more electrons are excited, which results in an increase in n, the number of electrons in the conduction band of TiO2 [31,33]. The open circuit voltage therefore increases. This observation is in agreement with our earlier report on the influence of concentration on anthocyanins on

electron transport in dye-sensitized solar cells. The difference here is that, in the present study, there is variation in the HOMO and LUMO of anthocyanins, which we now discuss together with their effects in the following paragraphs.

As explained earlier, when the pH is increased, (1) anthocyanins at approximately pH 7 appear to interact more favourably with TiO2, resulting in a more favourable pathway for electron injection into the conduction band of TiO2 [34]. (2) By raising the LUMO of the dye well above the conduction band edge of TiO2, a steep gradient is created that favours electron injection into the conduction band of TiO2 [31,33]. Figure 4 illustrates the band alignments of TiO2 and the dye at various pH values.

These two factors work synergistically and, in effect, result in an increase in n, the number of electrons in the conduction band of TiO2. Ideally, Eq. (2) approximates the open circuit voltage;

$$V_{oc} = E_{cB} - E_{ox} \qquad 2$$

The band gap of anthocyanins was investigated previously using cyclic voltammetry (CV) at pH 3.0, pH 3.5, pH 4.0, pH 4.5, pH 5.0, and pH 5.5 [28]. The band gaps obtained were 2.10, 2.16, 2.19, 2.23, 2.31, and 2.20, respectively. This clearly demonstrates that the bandgap of anthocyanins increases as the pH increases. The changes in band gaps were attributed to the changes in the position of the HOMO and LUMO of the dye as the pH was varied.

Another group of researchers investigated the effect of acidifying TiO2 on open circuit voltage [31]. While acidifying with nitric acid had no discernible effect on open circuit voltage, it is known from other research groups that acid treatment of TiO2 results in reduction of open circuit voltage. The reduction is attributed to the lowering of the conduction band edge of TiO2 [35,36].

The dyes were acidified with hydrochloric acid in this study, and TiO2 was dipped into the dyes. This equates to acidifying the anodes, and the explanation advanced thus far may still hold true. This probably explains why solar cells sensitized with more acidic anthocyanins have a lower open circuit voltage. It is thus worth noting that the open circuit voltage is indirectly dependent on the pH of the dye [23].

In contrast to our earlier study [9], it was not possible to discuss the variation in the alignment of the LUMO and HOMO of anthocyanins
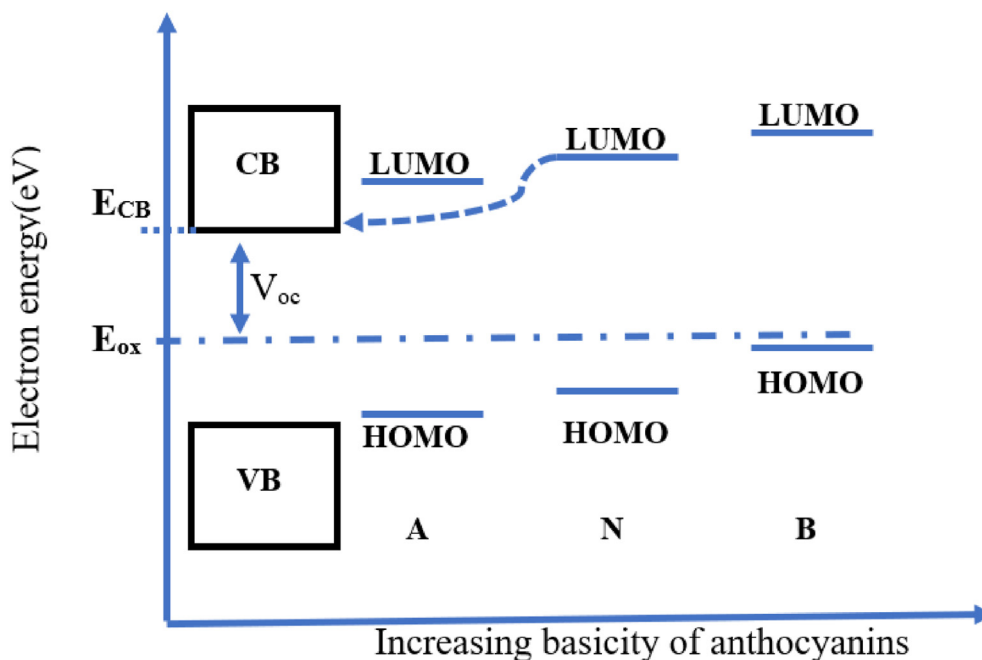
Figure 4. Scheme showing energy level alignments in dye-sensitized solar cells. CB: conduction band of TiO2, VB: valence band of TiO2, A: anthocyanin in acidic pH, N: anthocyanin with neutral pH, B: anthocyanin with basic pH, E_{CB}: conduction band edge of TiO2, E_{ox}: redox potential of the redox couple.
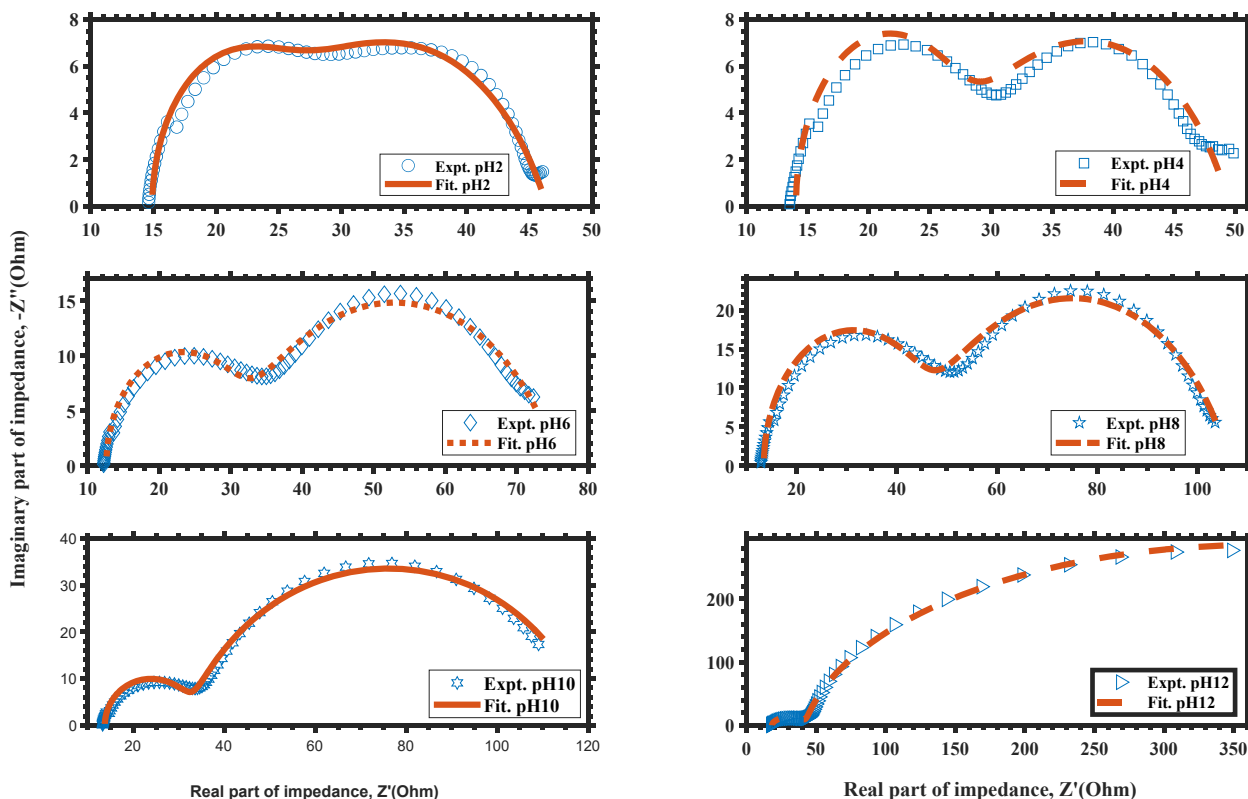
Figure 5. Nyquist plots of solar cells sensitized using anthocyanins at different pH values, at 0.70 V forward bias voltage, and in the frequency range of 1 Hz to 1 MHz.

relative to the conduction band edge of TiO_2 because we assumed that the LUMO and HOMO of the dye remain at a constant level for as long as the pH is constant. Additionally, it is worth noting that through investigation of the influence of pH on performance, the minimum conversion efficiency observed is 0.266% (pH 12), and the maximum is 0.390% (pH 8). This indicates an improvement of 46.62%. In contrast, when we varied the concentration of anthocyanins in our previous studies [9], the conversion efficiency had a minimum value of 0.065%, and a maximum value of 0.145%, an improvement of 123.08%. This means that by optimizing both the concentration and pH of anthocyanins, the performance of a dye-sensitized solar cell can be improved significantly.

3.3. Electrochemical impedance spectroscopy

Electrochemical impedance spectroscopy was used to further investigate the effect of the pH of anthocyanins on the performance of the solar cell. The Nyquist plots obtained at 0.70 V forward biased voltage in the frequency range of 1 Hz to 1 MHz are shown in Figure 5 together with the

simulated curves. The values of the circuit elements of Figure *1* obtained after simulation are presented in Table 2.

According to Table 2, both the charge transfer resistance, R3, at the anode and the chemical capacitance, C3, increase as the pH increases. To explain the increase, we turn to Eq. (3) [37], which defines the quasi-Fermi level.

$$E_F = E_{CB} - \frac{k_B T}{e} \ln \frac{n}{N_{CB}} \tag{3}$$

The quasi-Fermi level depends on n, which also depends on the recombination rate constant as well as on the number of injected electrons in the conduction band of TiO_2 [32,37]. Eq. (3) means that whenever n increases, E_F also increases [31]. The change transfer resistance at the anode and chemical capacitance of anode are related to Eq. (3) through equation (4) and equation (5) respectively [38, 39].

$$R = R_0 \exp\left[-\frac{\beta}{k_B T}(E_F - E_{redox})\right] \tag{4}$$

$$C_\mu = \frac{e^2}{k_B T} \exp\left[\frac{\alpha}{k_B T}(E_F - E_{CB})\right] \tag{5}$$

Table 2. Values of circuit elements used to simulate experimental data. R1: series resistance, R2: charge transfer resistance of the counter electrode, R3: charge transfer resistance of the anode, C3: chemical capacitance at the anode, Q: constant phase element at the cathode.

	R1 (Ω)	R2 (Ω)	Q2 (**F.s^n**)	n	R3 (Ω)	C3(**μ**F)
pH 2	14.66	22.81	46.02	0.67	8.95	5.57
pH 4	13.95	23.27	986.90	0.68	12.54	4.58
pH 6	12.50	46.27	812.40	0.68	17.62	6.02
pH 8	12.82	40.71	9.52	0.88	46.99	174.50
pH 10	13.06	24.57	37.30	0.81	71.50	33.00
pH 12	17.27	31.13	48.30	0.77	528.08	209.00

Table 3. Computed electron transport parameters; τ: electron lifetime, k_{eff}: recombination rate constant, n_s: electron density, and constant, Con.

	τ (μs)	k_{eff} (s^{-1})	Con. (Ω cms^{-1})	n_s (cm^{-3})
pH 2	49.85	2.00×10^4	170.05	9.49×10^{14}
pH 4	57.43	1.74×10^4	207.29	7.80×10^{14}
pH 6	206.35	0.01×10^4	256.06	6.30×10^{14}
pH 8	8199.76	0.01×10^4	5.45	2.96×10^{16}
pH 10	2346.82	0.04×10^4	0.29	5.58×10^{15}
pH 12	649.54	0.15×10^4	752.51	2.14×10^{14}
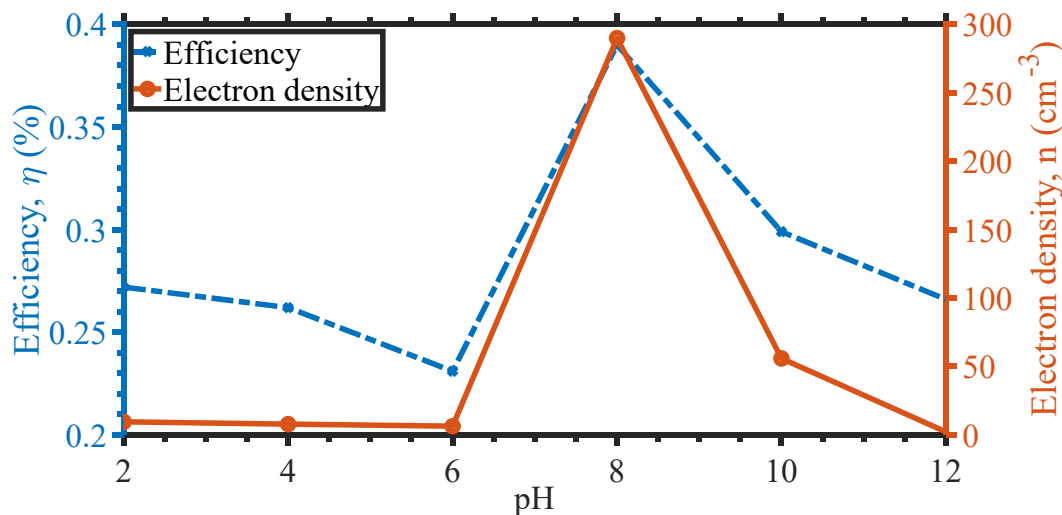
Figure 6. Graph showing the influence of electron density on solar conversion efficiency at varying pH of anthocyanins.

where E_F is the Fermi level of electrons, E_{redox} is the energy of the redox electrolyte, β is the transfer coefficient, R_0 is a constant, k_B is the Boltzmann constant, and T is the absolute temperature. E_{CB} is the energy of the conduction band, and α is a constant associated with the distributed energy states below the conduction band. When we substitute Eq. (3) into Eqs. (4) and (5) for E_F, we may thus conclude that the increase in charge transfer resistance and chemical capacitance is due to an increase in E_F in [34]. This observation is in agreement with our earlier studies [9], when the charge density increases. However, we stopped short of extending our studies to include the electron lifetime, recombination rate constant, and electron density. This limited our discussion of how electron density affects photovoltaic performance parameters. These are now addressed in the following paragraphs.

Using the results of Table 2; electron lifetime, τ; recombination rate constant, k_{eff}; constant, Con. And electron charge density, n_s, in the middle of TiO_2 were computed using equations (6) to (9), respectively [38, 39, 40, 41]. The computed parameters are presented in Table 3

$$\tau = R3 \times C1 \tag{6}$$

$$k_{eff} = 1/\tau \tag{7}$$

$$\text{Con.} = R3 \times l \times k_{eff} \tag{8}$$

$$n_s = k_B T / Aq^2 \times \text{Con.} \tag{9}$$

The electron lifetime is defined as the time an injected electron takes in the conduction band of TiO_2 before recombination occurs [22]. This parameter is observed to increase consistently up to pH 10. Thereafter, it drops in value. The trend of increasing electron lifetime is consistent with the increase in V_{oc} in Table 1. The impact of the changes in electron lifetime can also be viewed through the recombination rate constant, which is the inverse of electron lifetime. The recombination rate constants decrease from pH 2 to pH 10. This result is attributed to better dye interaction with the TiO_2 surface, which provides a better pathway for
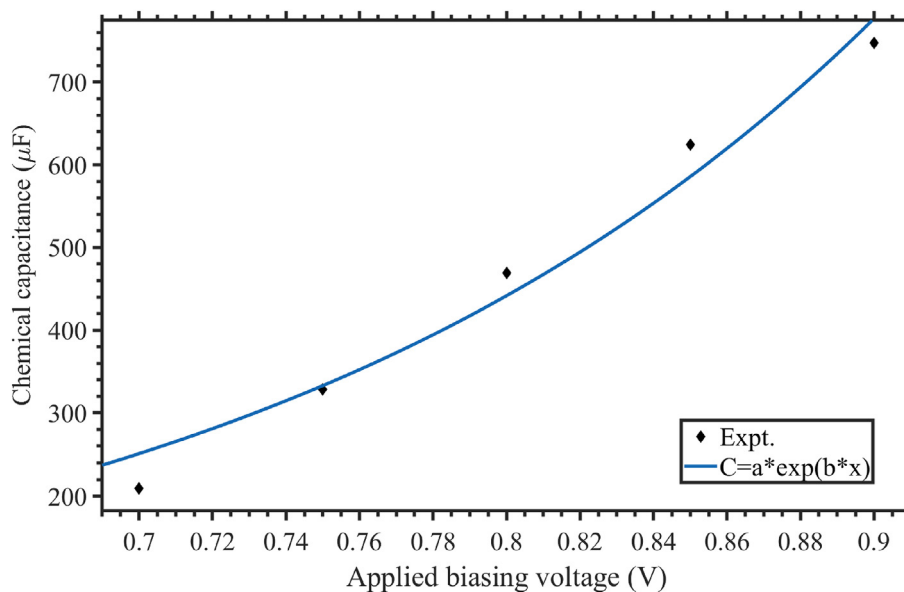
Figure 7. Graph of chemical capacitance against applied biasing voltage.

electrons from the dye to the conduction band of TiO_2 [32]. It has been reported that the type of anchorage between anthocyanins and the TiO_2 surface occurs through the bidentate anchoring mode [42]. The anchorage is usually through carbonyl and hydroxyl groups present in anthocyanins [43]. This occurs because of the condensation of alcohol-bound protons with the hydroxyl functional groups that are present on the surface of TiO_2 [43].

At pH 12, there is a significant increase in the recombination rate constant. This is probably due to the deattachment of dye molecules from the TiO_2 surface, which begins to occur at approximately pH 9 [3,44]. The deattachment makes more electrons available for recombination, as can be observed from the drop in current (Table 1).

The parameter con. is a function of the recombination rate constant through equation (8). It was used to compute charge density through equation (9). It can be observed that the trend of electron density in the conduction band is consistent with the trend of open circuit voltage. This highlights the effect of variation in electron density as a result of various molecular forms exhibited by anthocyanins in different pH environments.

The short circuit current and the solar conversion efficiency follows the trend set by the charge density. This is illustrated in Figure 6.

However, not all electrons injected in the conduction band contribute to the current. It seems that someelectrons end up in localized states [39, 45]. This argument can be supported by examining a graph of chemical capacitance at the anode against applied biasing voltage. Figure 7 is a sample graph of chemical capacitance, C against applied biasing voltage, V for the solar cell that was sensitized with anthocyanins at pH 12. The data points were fitted with the exponential Eq. (10)

$$C_\mu = a\, exp(bx); a = 4.812, b = 5.649 \qquad\qquad 10$$

The data points show an exponential increase in chemical capacitance as a function of applied biasing voltage. Such an increase is associated with the accumulation of charge in TiO_2 and in hole carriers [45]. Sharp spikes from the exponential increase are attributed to the presence of localized states in TiO_2 [22]. Such electrons transfer to holes in the redox carrier [22, 45].

4. Conclusion

Variation in pH anthocyanin (Cyanidin) leads to variations in the amount of light absorbed by anthocyanins at different pH values. The different amounts of light absorbed are attributed to different molecular forms of anthocyanins at different pH values. It was found that, as a result of variations in molecular forms at different pH values, the performance of sensitized anthocyanins also varied. The short circuit current decreased from pH 2 to pH 6. A maximum value of 0.399 mA was obtained at pH 8. It then decreases as basicity increases. The open circuit voltage increases consistently from pH 2 to pH 12. The solar conversion efficiency followed the same trend as the current. The maximum efficiency obtained was 0.390% at pH 8. Additionally, there was a 46.62% change from the minimum solar conversion efficiency to the maximum solar conversion efficiency. The improvement in performance at pH 8 was attributed mainly to the best interaction of the dye with TiO_2 at pH 8. EIS showed that recombination resistance and electron lifetime generally increase with increasing pH. It was also observed that as pH increases, there is an increase in electron density in the conduction band of TiO_2. Solar cells made with dyes at pH 8 had the highest solar conversion efficiency but the second largest electron density in the conduction band of TiO_2. This anomaly was attributed to the better interaction of the dye with TiO_2 at pH 8. In addition, the increase in electron density did not have a significant impact on the current. It was concluded that the majority of the electrons do not contribute to the current but are instead consumed by the oxidized electrolyte and excited dye. Being in the conduction band, however, causes a shift in the conduction band of TiO_2, hence increasing the open circuit voltage. Additionally, it is possible to improve the performance of dye-sensitized solar cells by optimizing the concentration of the sensitizing dye as well as its pH.

Declarations

Author contribution statement

Alex Okello: Conceived and designed the experiments; Performed the experiments; Analyzed and interpreted the data; Wrote the paper.

Brian Owino Owuor: Conceived and designed the experiments; Performed the experiments.

Jane Namukobe: Conceived and designed the experiments; Analyzed and interpreted the data; Wrote the paper.

Denis Okello: Analyzed and interpreted the data; Contributed reagents, materials, analysis tools or data; Wrote the paper.

Julius Mwabora: Analyzed and interpreted the data.

Data availability statement

Data will be made available on request.

Declaration of interests statement

The authors declare no conflict of interest.

Additional information

No additional information is available for this paper.

References

[1] N.T.R.N. Kumara, A. Lim, C.M. Lim, P.M. Iskandar, P. Ekanayake, Recent progress and utilization of natural pigments in dye sensitized solar cells:A review, Renew. Sustain. Energy Rev. 17 (2017) (2017) 301–317.

[2] P.P. Kumavat, P. Sonar, S.D. Dalal, An overview on basics of organic and dye sensitized solar cells, their mechanism and recent improvements, Renew. Sustain. Energy Rev. 78 (2017) (2017) 1262–1287.

[3] H.A. Maddah, V. Berry, S.K. Behura, Biomolecular sensitizers for dye sensititized solar cells: recent developments and critical insights, Renew. Sustain. Energy Rev. 121 (2020), 109678.

[4] N. Duvva, U. Chilakamarthi, L. Giribabu, Recent developments in tetrathiafulvalene and dithiafulvalene based metal-free organic sensitizers for dye-sensitized solar cells: a mini-review, Sustain. Energy Fuels 1 (678) (2017).

[5] H.A. Shittu, I.T. Bello, M.A. Kareem, M.K. Awodele, Y.K. Sanusi, O. Adedokun, Recent developments on the photoanodes employed in dye-sensitized solar cell, in: IOP Conference Series:Materials Science and Engineering, 2020.

[6] D. Rangel, J.C. Gallegos, S. Vargas, F. Garcia, Optimized dye-sensitized solar cells: a comparative study with different dyes, mordants and construction parameters, Results Phys. 12 (2019) 2026–2037.

[7] B. O'Regan, M. Gratzel, A low cost high efficiency solar cell based on dye sensitization colloidial titanium dioxide films, Nature 353 (1991) 737–740.

[8] T.V. Arjunan, T.S. Senthil, Review: dye sensitized solar cells, Mater. Technol. 28 (1&2) (2013).

[9] A. Okello, B.O. Owino, J. Namukobe, D. Okello, J. Mwabora, Influence of concentration of anthocyanins on electron transport in dye sensitized solar cells, Heliyon 7 (2021), e06571.

[10] A.N. Ossai, S.C. Ezike, P. Timtere, A.D. Ahmed, Enhanced Photovoltaic performance of dye sensitized solar cells based Carica papaya and black cherry fruit co-sensitizer, Chemical Physics Impact 2 (2021), 100024.

[11] S. Ananth, P. Vivek, T. Arumanayagam, P. Murugakoothan, Natural dye extract of lawsonia inermis seed as photo sensitizer for titanium dioxide based dye sensitized solar cells, Spectrochim. Actor Part A: Mol. Biomol. Spectro. 128 (2014) (2014) 420–426.

[12] H.M. Khalid, P.M. Firoz, M.N. Mia, A.A. Mortuza, M.S. Rahaman, M.R. Karim, J.M. Islam, F. Ahmed, M.A. Kham, Effect of dye extracting solvents and sensitization time on photovoltaic perfromance of photovoltaic dye sensitized solar cells, Results Phys. 7 (2017) 1516–1523.

[13] H. Setyawati, H. Darmokoesoemo, A.T. Ningtyas, Y. Kadmi, H. Elmsellem, H.S. Kasuma, Effect of metal ion Fe(III) on the performance of chlorophyll as photosensitizers on dye sensitized solar cell, Results Phys. 7 (2017) 2907–2918.

[14] M. Golshan, S. Osfouri, Azin Reza, T. Jalali, N.R. Moheimani, Co-sensitization of natural and low-cost dyes for efficient panchromatic light-harvesting using dye-sensitized solar cells, J. Photochem. Photobiol. Chem. 417 (2021) (2021), 113345.

[15] S. Tadesse, A. Abebe, Y. Chebude, I.V. Garcia, Y. Teketel, Natural dye sensitized solar cells using pigments extracted from syzigium guineense, J. Photon. Energy 2 (2012), 027001.

[16] C.Y. Chien, B.D. Hsu, Optimization of the dye-sensitized solar cell with anthocyanin as photosensitizer, Sol. Energy 98 (2013) (2013) 203–211.

[17] R. Byamukama, J. Namukobe, B. Kiremire, Anthocyanins from leaf stalks of cassava (Manihot esculenta cruntz), Afr. J. Pure Appl. Chem. 3 (2) (2009) 20–25.

[18] C. Adaku, I. Skarr, B. Helge, R. Byamukama, M. Jordheim, A.M. Oyvind, Anthocyanins from mauve flowers of Erlangea tomentosa (Bothriocline longipes) based on erlangidin – the first reported natural anthocyanidin with C-ring methoxylation, Photochemistry Letters 29 (2019) 225–230.

[19] J. Namukobe, Analysis of Anthocyanins from Fruits of Lea Guineensis and Flowers of acanthus Pubscence, 2006.

[20] S. Hao, J. Wu, Y. Huang, J. Lin, Natural dyes as photosensitizers for dye sensitized solar cells, Sol. Energy 80 (2006) 209–2014.

[21] R.V. Gomez, S.D. Jimenez, A.F. Mato, Z.A. Lara, R.T. Bonilla, M. Courel, Recent advances in dye sensitized solar cells, Appl. Phys. A 125 (836) (2019).

[22] V. Odari, R. Musembi, J. Mwabora, Enhanced performance of Sb2S3 mesoscopic snesitized solar cells employing TiO2:Nb compact layer, Mater. Sci. Electron. (2018) 16359–16368.

[23] X. Yin, Y. Guo, Z. Xue, P. Xu, M. He, B. Liu, Enhance the Performance of Perovskite-Sensitized Mescopic Solar Cells by Employing Nb Dopped TiO2 Compact Layer, Nano Research, 2015.

[24] G. Boschloo, Improving the performance of dye-sensitized solar cells, Cells.Front.Chem 7 (77) (2019).

[25] A. Omar, M.S. Ali, N.A. Rahim, Electron transport properties analysis of titanium dioxide dye-sensitized solar cells (TiO2-DSSCs) based natural dyes using electrochemical impedance spectrocopy concept, Sol. Energy 207 (2020) (2020) 1088–1121.

[26] H. Wang, P. Li, W. Zhou, Dyeing of silk with anthocyanins dyes extract from liriope platyphylla fruits, J. Textil. 2014 (2014) 9.

[27] N.Y. Amogne, A.W. Delele, T.A. Yeshitila, Recent advances in anthocyanins dyes extracted from plants for dye sensitized solar cells, Mater. Renew. Sustain. Energy 9 (23) (2020).

[28] S. Suyitno, T.J. Saputra, A. Supriyanto, Z. Arifin, Stability and efficiency of dye-sensitized solar cells based on papaya-leaf dye, Spectrochim. Acta Part A: Mol. Biomol. Spectro. 148 (2015) 99–104.

[29] S.A. Mahmoud, H. Atia, H.S. Bendary, Synthesis of a high efficiency novel working electrode scandium/HOMBIKAT in dye-sensitized solar cells, Sol. Energy 2016 (134) (2016) 452–460.

[30] T. Shoji, Polyphenols as natural food pigments:Changes during food processing, Am. J. Food Technol. 2 (7) (2007) 570–581.

[31] R. Katoth, A. Furube, Electron injection efficiency in dye-sensitized solar cells, J. Photochem. Photobiol., A C 20 (2014) 1–16.

[32] Z. Ning, Y. Fu, H. Tian, Improvement of Dye-Sensitized Solar Cells: what We Know and what We Need to Know, The Royal Society of Chemistry, 2010, pp. 1170–1181.

[33] R.R. Sonia, E.M. Barea, S.F. Fabregat, Analysis of the origin of open circuit voltage in dye solar cells, J. Phys. Chem. Lett. 3 (2012) 1629–1634.

[34] B. Kim, S.W. Park, J.Y. Kim, K. Yoo, J.A. Lee, M.W. Lee, D.K. Lee, J.Y. Kim, B. Kim, H. Kim, S. Han, H.J. Son, M.J. Ko, Rapid Dye Adsorption via Surface Modification of TiO2 Photoanodes for Dye-Sensitized Solar Cells, Applied materials and interfaces, 2013.

[35] B. O'Regan, M. Gratzel, D. Fitzmaurice, Optical electrochemistry I:steady-state spectroscopy of conduction-band electrons in a metal oxide semiconductor electrode, Chem. Phys. Lett. 183 (1) (1991), 2.

[36] R. Flood, B. Enright, M. Allen, S. Barry, A. Dalton, H. Doyle, D. Tynam, D. Fitzmaurice, Determination of band edge energies for transparent nanocrystalline TiO2-CdS sandwich electrodes prepared by electrodeposition, Sol. Energy Mater. Sol. Cell. 39 (1995) 83–98.

[37] S.A.A. Syed, M.H. Sayyad, N. Nasr, R.A. Toor, S. Sajjad, H. Elbohy, Q. Qiao, Photovoltaic performance and impedance spectroscopy of a purely organic dye and most common metallic dye based dyesensitized solar cells, J. Mater. Sci. Mater. Electron. (2017).

[38] F.F. Santiago, J. Bisquert, E. Palomares, D. Kuang, S.M. Zakeeruddin, M. Gratzel, Correlation between photovoltaic performance and impedance spectroscopy of dye sensitized solar cells based on ionic liquids, J. Phys. Chem. C 6550–6560 (2007) 111.

[39] S.N. Zaine, N.M. Muhamed, M. Khatani, A. Eskandar, M.U. Shahid, Trap state and charge recombination in nanocrystalline passivated conductive and photoelectrode interface of dye-sensitized solar cell, Coatings 10 (284) (2020).

[40] M. Adachi, M. Sakamoto, J. Jiu, Y. Ogata, I. Seiji, Determination of parameters of electron transport in dye sensitized solar cells using electrochemical impedance spectroscopy, J. Phys. Chem. B 110 (2006) 13872–13880.

[41] J. Halme, P. Vahermaa, k. Miettunen, P. Lund, Device physics of dye solar cells, Adv. Mater. 22 (2010) E210–E234.

[42] C.D. Uribe, W. Vallejo, E. Romero, M. Villareal, M. Padilla, N. Hazbun, A.M. Acevedo, E. Schott, X. Zarate, TiO2 thin films sensitization with natural dyes extracted from Bactris guineensis for photocatalytic applications: experimental and DFT study, J. Saudi Chem. Soc. 2020 (24) (2020) 407–416.

[43] R. Ramamoorthy, K. Karthika, A.M. Dayana, V. Maheswari, N. Pavithra, S. Anandan, R.V. Williams, Reduced graphene oxide embedded titanium dioxide nanocomposite as novel photoanode material in natural dye-sensitized solar cells, J. Mater. Sci. Mater. Electron. 28 (2017) 13678–13689.

[44] H.A. Maddah, V. Berry, S.K. Behura, Biomolecular sensitizers for dye sensitized solar cells: recent developments are critical insights, Renew. Sustain. Energy Rev. 121 (2020) (2020).

[45] F.F. Santiago, G.G. Belmonte, I.M. Sero, J. Bisquert, Characterization of nanostructured hybrid and organic solar cells by impedance spectroscopy, Phys. Chem. Chem. Phys. 13 (2011) 9083–9118.